As featured in:

Soft Matter

Themed issue: Liquid composites

ROYAL SOCIETY OF CHEMISTRY

See Rebecca Kramer-Bottiglio *et al.*, *Soft Matter*, 2020, **16**, 5827.

ROYAL SOCIETY OF CHEMISTRY

rsc.li/soft-matter-journal

Uniform conductivity in stretchable silicones *via* multiphase inclusions†

R. Adam Bilodeau, [ID] ‡[ab] Amir Mohammadi Nasab, [ID] ‡[a] Dylan S. Shah [ID] [a] and Rebecca Kramer-Bottiglio [ID] *[a]

Many soft robotic components require highly stretchable, electrically conductive materials for proper operation. Often these conductive materials are used as sensors or as heaters for thermally responsive materials. However, there is a scarcity of stretchable materials that can withstand the high strains typically experienced by soft robots, while maintaining the electrical properties necessary for Joule heating (*e.g.*, uniform conductivity). In this work, we present a silicone composite containing both liquid and solid inclusions that can maintain a uniform conductivity while experiencing 200% linear strains. This composite can be cast in thin sheets enabling it to be wrapped around thermally responsive soft materials that increase their volume or stretchability when heated. We show how this material opens up possibilities for electrically controllable shape changing soft robotic actuators, as well as all-silicone actuation systems powered only by electrical stimulus. Additionally, we show that this stretchable composite can be used as an electrode material in other applications, including a strain sensor with a linear response up to 200% strain and near-zero signal noise.

1 Introduction

Soft robotic technologies have achieved increasing success in a wide range of actuation domains including robotic grippers,[1,2] wearable assistive devices,[3–5] and robot arms.[6] Simultaneously, stretchable electronics have shown success in a variety of use cases, including as biocompatible devices,[7,8] wearable technologies,[5,9] and, of course, soft robotic electronics.[10,11] Though there are many ways to create mechanically compliant stretchable electronics (patterning, printing, *etc.*),[12,13] within the context of soft robots it is often architecturally simpler to embed conductivity into a bulk stretchable material that matches the material compliance of the other soft robot components.[14] Recently, researchers have integrated stretchable, electrically conductive materials into soft robots to add sensing,[15] heating,[16,17] or signal and power lines,[18] while reducing manufacturing complexity of the overall system.[19]

To create high-strain, bulk conductive composites, many groups have embedded rigid conductive inclusions into stretchable materials. Only a few of these types of composites can handle linear strains of up to 100%,[14,20] and those composites often require specialized composite filler materials with complex manufacturing techniques[21,22] or require specialized rubbers.[23] Even so, conductive composites can be used for electrical signaling and sensing, but when their conductivity is not spatially uniform under strain, they experience uneven energy dissipation while Joule heating, creating "hot spots" in the material. This non-uniform conductivity prevents them from being an embedded heat source for thermally triggered soft robotic components, such as volumetrically expanding silicones,[24,25] stiffness-varying stretchable silicones,[26] and liquid crystal elastomer actuators.[27] In a recent work, we showed that adding expanded intercalated graphite (EIG)[28] into a silicone matrix in high enough concentrations (>7 vol%) creates a composite with uniform electrical conductivity capable of Joule heating up to 150 °C.[29] However, due to the high quantity of stiff EIG inclusions, the composite could not be stretched higher than 40% strain without cracking internally, creating thermal hot spots for Joule heating (although the material retained its electrical conductivity).

To improve material performance beyond the current limits of rigid inclusions, we draw on principles from a new class of liquid metal embedded elastomers (LMEEs). LMEEs are made by mechanically mixing a room temperature liquid metal (eutectic gallium–indium, or eGaIn) into uncured silicone at high volumetric ratios (>30%), which creates a highly-stretchable thermally-conductive composite that maintains the elastomer's mechanical properties, while often improving other characteristics, such as dielectric strength and thermal conductivity.[30–32]

[a] Department of Mechanical Engineering and Materials Science, School of Engineering and Applied Science, Yale University, 9 Hillhouse Ave., New Haven, CT 06511, USA. E-mail: rebecca.kramer@yale.edu
[b] School of Mechanical Engineering, Purdue University, 585 Purdue Mall, West Lafayette, IN 47907, USA
† Electronic supplementary information (ESI) available. See DOI: 10.1039/d0sm00383b
‡ These authors contributed equally to this work.

Although non-conductive as cast, LMEEs easily integrate with other elastomers to improve current soft robotic actuator technologies.[33,34]

LMEEs can be activated using mechanical "sintering" techniques which cause the liquid metal inclusions to flow together and create channels with high electrical conductivity.[18] Sintering has been achieved by applying localized pressure on the composite[18,27] and freezing the system to simultaneously activate the entire composite.[35] Hybrid composites exist in which liquid metal and a solid conductor are blended in the same silicone to create a composite that is conductive as-cast.[36–38] So far this has been primarily to use the liquid metal to enhance the functionality of the solid conductive filler, as evidenced by low volume fractions of liquid metal. Wang *et al.*, recently reported a high strain elastomer composite (>700%) using rigid particles and liquid metal inclusions,[39] but the composite requires over 1000 cycles to stabilize its resistance, and exhibited relatively low conductivity compared with other liquid metal-silicone composites.[40,41]

In this paper, we show that the addition of a small amount of rigid EIG filler enables highly stretchable LMEEs to self-activate, becoming highly conductive and Joule heating-capable composites. This novel multiphase composite (MPC) self-activates under high linear strains (>200%), which drops its electrical resistivity by up to five orders of magnitude to $<4 \times 10^{-5}$ Ω m. The MPC maintains a uniform, low resistivity while undergoing 200% linear strain, even when cycled 10 000 times. MPC silicone can be used in a wide range of applications, including Joule heating (Fig. 1) and strain sensing. We show that, because of its high deformation capability, MPC silicone is highly compatible with other new soft robotic silicone composites and enables the creation of solid-state soft actuators that are robust to damage, and multifunctional thin film pneumatic bladders that can dynamically change their trajectory while providing sensory feedback. With its high conductivity and high strain capacity, MPC silicone is a step towards versatile soft robotic

Fig. 1 An activated 4 × 16 cm sample of the MPC being simultaneously twisted and stretched, while maintaining a consistent, uniform Joule heating profile. The sample is fully encapsulated in silicone.

components which can change their shape and sense their deformations, using the same material.

2 Principles of operation

MPC silicone has three main components: eGaIn as the liquid metal (LM) alloy; EIG as the rigid conductive filler; and silicone elastomer (SE) as the composite matrix. In brief, it is manufactured by shear mixing 60% LM with 40% SE by volume, and then adding 1% vol EIG filler to the mixture (additional details in Materials and methods). As cast, the EIG fillers bridge the LM particles in the silicone matrix. This means the material is electrically conductive while also being stretchable up to ~100% strain, although it has a high electrical resistivity (1.28 ± 0.57 Ω m).

To activate the composite and increase its electrical conductivity, the material is strained to such a degree that the silicone matrix tears locally, allowing the LM inclusions to flow and coalesce into a low resistance network percolating throughout the composite (see Videos S1 and S2, ESI†). This strain-based activation requires the MPC to be supported by an extensible backing layer that adheres to the MPC to prevent catastrophic failure, by absorbing some of the energy released when the matrix tears. The supportive backing layer can be another silicone layer or even a stretchable adhesive tape (3M VHB tape) which is removable after activation (Fig. S1, ESI†). Most of the samples in this paper use some form of silicone backing layer, to improve mechanical robustness and facilitate the addition of electrodes.

Thrasher *et al.*, recently demonstrated a similar strain-activated mechanism in so-called "polymerized liquid metal networks".[42] Acrylate ligands were bound to the surface of liquid metal particles, then cast and polymerized together, forming a 99% LM particle film on a substrate. Similar to the mechanism shown here, strain caused the initially isolated LM particles to rupture, allowing the liquid metal cores to flow and coalesce into a percolating conductive network. Our work differs from this in that we use a lower concentration of liquid metal, and our silicone matrix is typically more compatible with other traditional materials used in soft robots.[43]

To demonstrate MPC silicone's activation mechanism, we compared the activation (*i.e.*, first-strain behavior) of a LM–SE–EIG composite with that of LM–SE and SE–EIG composites (Fig. 2). When 60% LM and 40% SE by volume are shear-mixed and cured (Fig. 2a–c, left column), the material is neither electrically conductive as cast, nor after being stretched, even with the high volume fraction of conductive LM. With no internal stress concentrators (*i.e.*, rigid particles) to incite microscopic failures in the silicone matrix, the liquid metal cannot coalesce into a conductive network. When 90% SE is mixed with 10% EIG by volume (Fig. 2a–c, middle column), the material is electrically conductive as cast, but also comparatively brittle (failure at 40% strain) due to the rigid inclusions. When the two composites are combined to create LM–SE–EIG composite, the MPC silicone develops a uniform distribution of
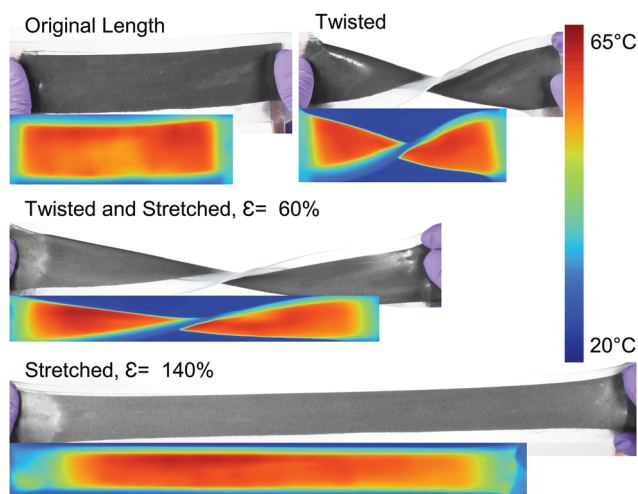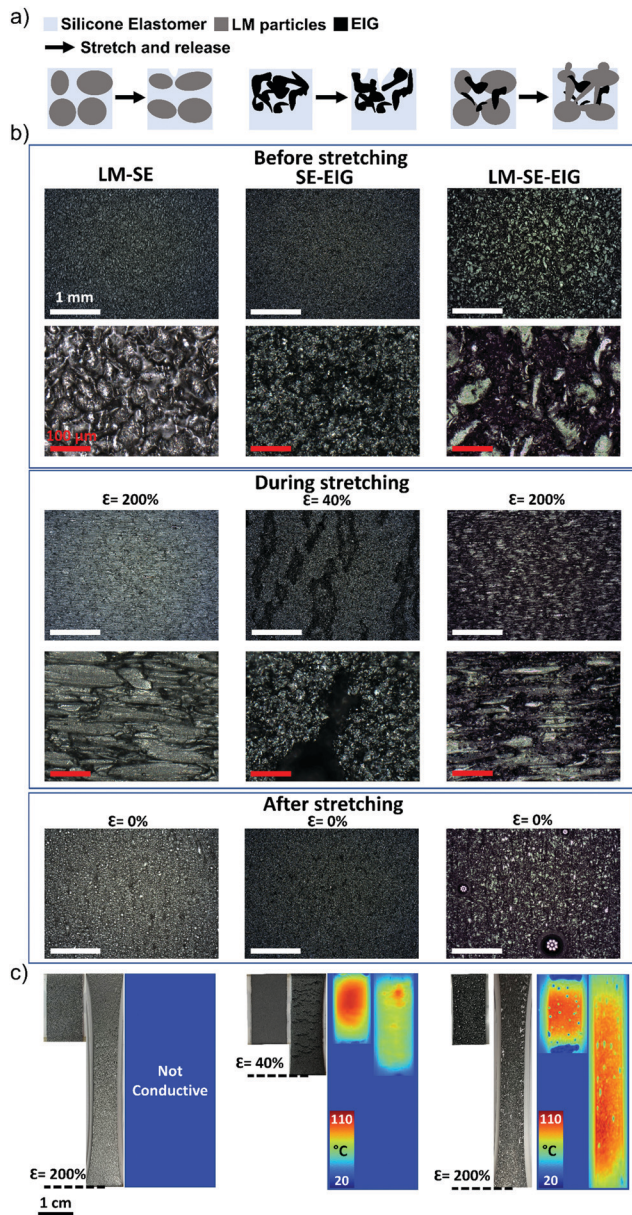
Fig. 2 Principles of operation of the MPC. (a) Schematic compares pre- and post-stretch structures of three composite materials of LM–SE,[30,44] SE–EIG,[29] and LM–SE–EIG (left to right). In the left column, although some microcracks appear on the surface of the LM–SE composite while being stretched, a conductive pathway through the whole structure does not form. In the middle column, the majority of conductive pathways in the SE–EIG composite are lost due to macroscopic cracks forming in the material. In the right column, the EIG facilitates microcracks in the LM–SE–EIG composite during stretching, which creates conductive pathways throughout the structure (activation). (b) mm- and µm-scale images show the surface features of the three composites as cast, while stretched, and relaxed post-stretch. Light reflections from the microscope are visible on the LM beads expelled from the LM–SE–EIG surface. (c) Optical and thermal images of samples of the three aforementioned composites Joule heated with electrical current at rest and stretched states, after a one-time 'activation' event. Temperature variance is used to view the resistance uniformity, as higher resistance areas generate more heat when a current is passed through the system.

microcracks both internally and visibly on the surface after stretch (Fig. 2a–c, right column). The LM particles coalesce through these pathways creating a continuous conductive network (seen as reflective pools forming at the microcrack sites, visible in Video S2, ESI†), uniformly lowering the resistivity by several orders of magnitude. Additional evidence of a continuous internal liquid metal network is presented in Fig. S2 (ESI†), where liquid metal drains out the bottom of a vertically-oriented MPC sample over a period of 40 minutes.

Fig. 2b presents optical images of the surface of the three composite structures pre- and post-stretch. In the LM–SE composite (left column), LM particles maintain their boundaries, even at 200% strain. Some minor microcracks form on the surface of the LM–SE composite, but these are insufficient to create a conductive pathway through the whole structure (Fig. 2c, left). This same microscale robustness holds when the LM–SE composite is compressed, a technique used in other works to create conductive pathways using silicones with lower yield strains.[18] In contrast, the SE–EIG composite exhibits brittle behavior from macrocracks on the surface when stretched to only 40% strain (Fig. 2b, middle column). These cracks cause a rapid rise in the electrical resistance of the structure and a non-uniform electrical conductivity (Fig. 2c, middle). Neither of these composite mixtures generate the desired high stretchability with uniform conductivity that is shown in our final MPC mixture.

Combining the fillers for the two non-functioning composites, microcracks are formed in the LM–SE–EIG silicone matrix when stretched (Fig. 2, right column), resulting in a low, uniform electrical resistivity (Fig. 2c, right). When released, some LM inclusions are displaced from inside the system and LM beads form on the surface of the MPC (Video S2, ESI†), a phenomenon previously observed in other strain-activated liquid metal composites.[42] We hypothesize that the displaced LM is due to the plastic deformation of the MPC (see Fig. S1, ESI†) relative to the elastic deformation of its backing layer during strain, which induces buckles and wrinkles throughout the MPC when relaxed.[45] Such wrinkling is visible in Fig. 2b and Video S2 (ESI†), and explains the displaced volume of LM during strain activation. To aid in transporting or attaching the MPC to another material system, we simply remove the excess LM beads by gently wiping the surface of the material with a cloth infused with Simple Green (Sunshine Makers, Inc) or another acidic or basic cleaning agent.

Fig. 2c shows 10 × 20 mm samples of three composites at rest and in stretched states while they were Joule heated. MPC silicone shows a uniform temperature distribution on its surface as an indication of uniform electrical conductivity. Note that cool spots on the thermal image are not actually lower in temperature. They are the LM surface beads causing the IR camera to misreport their temperature as cooler, since LM has a lower emissivity than silicone.

3 Material characterization

As previously noted, the primary MPC mixture we use is initially mixed to 60% LM and 40% SE by volume, with subsequent

addition of 1% EIG by volume (suspended in cyclohexane as a carrier solvent). Although this makes a composite that is 59.4%–39.6%–1%, we use a shorthand convention to simplify notation, as 60–40–1. This notation is used for all other mix ratios tested.

3.1 Electrical and mechanical properties

Volume fractions of LM and EIG were varied in the MPC compositions to investigate their role in the electrical conductivity of MPC silicone (Fig. 3). For the tests evaluating the electrical resistivity, the MPC samples were supported with a pure silicone backing layer. Fig. 3a shows the electrical resistivity of the activated (post-stretch) samples of MPC silicone for various volume fraction of LM and EIG. The electrical resistivity ρ, was calculated by measuring the electrical resistance R, thickness t, length l, and width w of MPC silicone samples using $\rho = R(tw)/l$.

As volume fractions of LM or EIG increased, the electrical resistivity of the MPC decreased. We found that there is a lower-limit to filler concentrations that, if the combination of LM and EIG is too low, the material does not activate (black pyramids in Fig. 3a). If the material is filled with 60% LM volume fraction, even adding just 0.5% EIG will make the MPC electrically conductive. This concentration is close to the theoretical upper limit based on the maximum packing fraction in a randomly dispersed 3D mixture for fillers with aspect ratio close to one (about 64%[46]). Since the LM does not have an aspect ratio of exactly one, it might be possible to increase the concentration beyond 60% LM, but we discovered that any more LM made the materials very difficult to mix together uniformly.

Fig. 3a shows that for compositions with LM volume fraction of 50%, increasing the EIG content from 1% to 2% decreased the electrical resistivity of the MPC after activation by 66%. However, for MPC compositions with LM volume fraction of 60%, that same increase in EIG content only decreased the electrical resistivity of the MPC by 22%. This indicates that the EIG, as a conductive filler, contributes relatively little to the material's activated conductivity for compositions with a high (>50%) LM volume fraction.

Fig. 3b and c is a before and after comparison of the electrical resistivity of MPC silicone for various material compositions. Varying the volume fraction of EIG in the MPC, the resistance drop after activating the material is 5, 4, and 3 orders of magnitude for 60–40–0.5, 60–40–1, and 60–40–2 compositions, respectively (Fig. 3b). Notably, the electrical resistivity of the activated 60–40–1 composition is about one order of
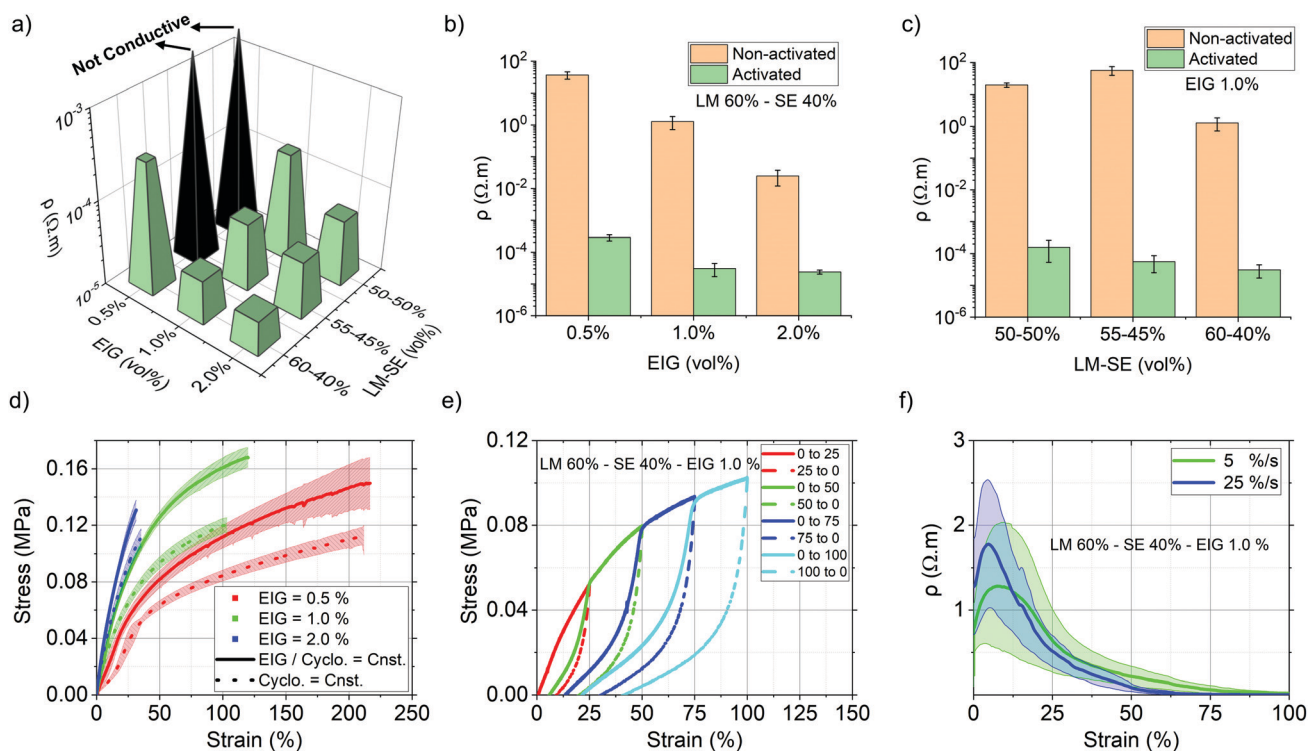

Fig. 3 Electrical and mechanical characterization of MPC silicone. (a) Electrical resistivity of the MPC after stretch as a function of LM and EIG volume fractions. Truncated pyramids show the compositions with electrical conductivity and full pyramids show the non-conductive compositions. (b and c) Electrical resistivity of MPC silicone pre- and post-activation. (b) LM 60%–SE 40% composition, varying the EIG volume fraction. (c) EIG 1% composition, varying the LM–SE volume fraction. (d) Mechanical testing of unactivated MPC (LM 60%–SE 40%, no backing layer), with 0.5%, 1.0%, and 2.0% volume fractions of EIG showing the elongation at break. (e) Cyclic loading of MPC silicone (LM 60%–SE 40%) with 1.0% volume fraction of EIG. The material displays a Mullins effect at the first loading cycle at each strain. The stress is significantly smaller in the next cycles at the same strain level. (f) Activation process of the MPC at two strain rates of 5% s^{-1} and 25% s^{-1}. Five samples at each speed are stretched up to 250% strain for the first time and the resistivity change is recorded. The material begins activating at lower strains when stretched with a higher strain rate. A representative plot of resistance drop for a sample is shown in Fig. S3 (ESI†). Error bars in (b and c), and shaded regions in (d and f) represent ±1 standard deviation.

magnitude lower than that of the activated 60–40–0.5 composition. This notable drop in electrical resistivity is likely due to an increase of microcrack nucleation sites in the composite matrix from the increased EIG content (rather than a direct result of the EIG being conductive) enabling an improved LM network in the final, activated composite. The pre- and post-activation electrical resistivity of different MPC compositions with varying LM concentrations and 1% EIG is shown in Fig. 3c, with a more gradual downward trend in the resistivity as LM concentration increases.

It has been shown that solvents trapped in silicones can influence mechanical properties.[47] Cyclohexane is a relatively volatile solvent and it evaporates during the process of mixing the material and casting it into thin sheets. However, a small amount of solvent still evaporates after the MPC is cured leaving some voids behind in the structure of the composite. To investigate the effect of the EIG carrier solvent (cyclohexane) volume fraction on the mechanical properties of the MPCs, evaluations were performed for two mixture 'recipes': (1) the ratio of EIG to cyclohexane kept constant while the EIG content is varied in the mixture, and (2) the volume fraction of cyclohexane kept constant in the mixture disregarding variations in the EIG content, which resulted in a higher fraction of cyclohexane to silicone in the uncured mixture. Fig. 3d shows the tensile mechanical behavior of unactivated MPC silicone samples (with no backing layer) for compositions 60–40–0.5, 60–40–1, and 60–40–2 as samples were stretched to failure. Increasing the EIG volume fraction in the composition increases the elastic modulus and decreases elongation at break. In the first recipe, MPC silicone with 0.5%, 1.0%, and 2.0% EIG volume fractions break at 216%, 120%, and 31% strain, respectively. For the second recipe, the elongation at break is only slightly lower at each composition, although the elastic modulus is reduced, as expected.[47] These observations support our hypothesis that elongation at break is strongly dependent on EIG content after curing and only weakly dependent on the solvent content during mixing. Additionally, the ultimate strains recorded here provide minimum strains required to begin activation of each material composition such that there will be internal microcracking, and demonstrate the need for the backing layer (so the system can stretch to 250%) during activation.

MPC silicone displays a Mullins effect at the first loading cycle to an elevated strain value (Fig. 3e). The stress is significantly smaller in the next cycles at the same strain level. This response to the initial loading is expected in liquid-composite elastomers,[30] as it is observed in most elastomers. If the MPC is stretched to the same strain after the first loading, the Mullins effect disappears, but returns if the MPC is stretched more than its previous maximum strain.

MPC silicone also exhibits viscoelastic properties (*i.e.*, strain rate dependencies), as would be expected by a silicone elastomer system. This viscoelasticity results in higher stresses in the composite when the material is strained at higher rates, triggering the nucleation of microcracks at lower strain levels. Therefore the MPC activates at a lower strain level when stretched at a higher strain rate, as shown in Fig. 3f. Fig. S3 (ESI†) shows the representative resistance–strain activation curve for a single sample strained up to 250% strain.

Among all the compositions evaluated in Fig. 3, 60–40–1 and 60–40–2 MPC silicone compositions always result in uniform electrical conductivity when strained to 250% strain. We suspect the reason to be that the increased volume fraction of LM increases the statistical uniformity of the distribution of LM inclusions, as well as their local proximity to each other. This uniform distribution of inclusions, combined with slightly elevated quantities of EIG, likely ensures that there is simultaneous microcracking throughout the composite during activation. We note that other factors influence the uniform conductivity of the MPC as well. Such factors include constant sample thickness, activation strain value (mature *vs.* premature activation), and uniformity of the activation strain field, as shown in Fig. S4 (ESI†). We chose a 60–40–1 MPC silicone composition for the applications shown in the paper, to keep uniform electrical conductivity after activation.

3.2 Thermal characteristics and cyclic robustness

Conductive silicone composites have been previously used as Joule heaters, trading off between high temperature-change capabilities[48] or improved stretchability.[16,17,29,49] In order to be easily integrated into soft robots, desired properties include high temperature change capability, stretchability, and uniform resistivity (leading to uniform heating capabilities). Here we aim to quantify the suitability of the MPC as a heater material, while identifying potential limitations and advantages of our material.

Specifically, we used 60–40–1 MPC silicone as a heater, and evaluated its thermal response to different electrical inputs. Fig. 4a shows the surface temperature of a 40 × 10 × 0.4 mm MPC sample supported with a 1 mm thick silicone backing layer. The initial resistance of the sample at 0% strain was 1 Ω. The sample was stretched to 100 and 200% strain and still demonstrated a uniform heat distribution over its surface, though the resistance increase caused the maximum achievable temperature at a fixed electrical current input (2.5 A) to decrease. Reducing the thickness of the backing layer allows the material to heat up faster, since there is less mass to absorb the thermal energy. An example is shown in Fig. S5 (ESI†), in which an activated MPC silicone and its silicone backing layer have a total thickness of less than 250 μm.

To further characterize MPC silicone's robustness as a heater, we coated neat silicone on both sides of 30 × 10 × 0.4 mm MPC samples and cycled them 10 000 times to 200% strain. In Fig. 4b we show electrical resistance over the whole test on one sample, with an initial settling in the resistance for 300 cycles followed by a plateau in the sample's resistance. Mechanical strength after 10 000 cycles was observed to be similar to the original material, consistent with prior work in which robust cyclic mechanical testings have been performed on similar materials.[28,33] IR images of the sample Joule heated at 0 and 200% strain with 2.2 A electrical current is displayed in Fig. 4c, showing negligible difference in heating performance of the sample before and after the cyclic test.
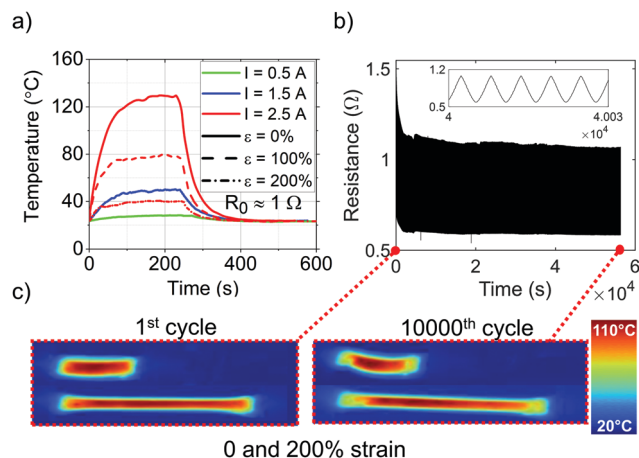
Fig. 4 Thermal characteristics and cyclic robustness. (a) Temperature of a 40 × 10 × 0.4 mm activated MPC silicone sample supported with a 1 mm thick backing layer while being Joule heated with 0.5 A, 1.5 A, and 2.5 A for four minutes at 0% strain. The sample was then allowed to cool for six minutes at room temperature. Additionally overlaid is the same sample heated with 2.5 A at 100% and 200% strain. (b) Resistance change of a MPC silicone sample (30 × 10 × 0.4 mm) cycled 10 000 times to 200% strain. Inset shows 30 s of cycling. (c) IR images of the sample heating up with electrical current of 2.2 A before and after the cyclic test, showing no visible decrease in uniformity inside the main body.

We performed additional cyclic tests on samples that were coated with only a single backing layer of neat silicone (*i.e.*, 'one-sided' backings). These samples could only achieve 10 000 cycles if the strain was reduced to 150% (Fig. S6, ESI†). If they were strained cyclically to 200%, the one-sided samples would fail between 3000 and 5000 cycles. We therefore conclude that the highest cyclic performance is enabled by coating neat silicone on both sides of the MPC, which agrees with more detailed investigations done in prior work.[29]

4 Applications

In the previous experiments, we have shown that MPC silicone can be used to make planar, skin-like sheets with high stretchability and uniform conductivity. We now use the material as a key component in three distinct systems, achieving multiple functions while reducing system complexity. The first application leverages the high conductivity of the MPC to enable high-strain sensory feedback with low noise. We then apply the MPC as a "skin" around a solid silicone composite that increases in volume when heated, producing a solid-state, all-soft actuator. Finally, we integrate it into the walls of a pneumatically inflating bladder with thermally controlled stretchability, allowing a single-bladder pneumatic actuator to attain multiple motion trajectories *via* electrical stimulus, all while using the MPC to simultaneously measure the actuator's state.

4.1 High deformation sensing

We used activated 60–40–1 MPC silicone to create capacitive strain sensors which exhibit a repeatable linear response over strains as high as 200%. Capacitive strain sensors have been

deployed in numerous applications ranging from measuring human body motion,[50,51] reconfigurable robotic skins,[52] robot grippers,[19] and numerous other applications.[53,54] The classic 3-layer design (used in this work) has stretchable planar electrodes on the top and bottom of a stretchable dielectric material. Capacitive sensors provide a more consistent response than resistive sensors, where comparisons between the capacitance and resistance of sensors of the same material are available.[28,50] Measuring the capacitance of such sensors (typically on the order of 1–100 pF) is a challenging task however, and several methods have been employed.[55] Each proposed method has benefits and drawbacks, but generally low electrode resistance and high capacitance are desirable, giving our new MPC silicone an opportunity to improve current sensor systems.

One drawback to capacitive sensing methods is that they are relatively susceptible to external noise. Noise can come from many sources, including an unstable ground or supply line. Additionally, the sensor will pick up external electromagnetic noise in the form of an unstable electrode voltage and correspondingly noisy capacitance measurements. Filtering can be used to mitigate the effects of such noise, for example using analog low-pass filters,[56] or using digital signal processing methods (as is done on the MPR121, manufactured by NXP Semiconductor). Here, we found that our sensor paired with the MPR121 results in a stable system, with resting noise standard deviation σ of only $\sim$0.05% of the full scale range of the sensors' response over 200% strain, or σ = 0.1% (further analysis presented in ESI† as Table S1).

To investigate the advantages and disadvantages of various combinations of sensors and sensing circuits, we compared the MPC sensors to SE–EIG sensors[28] (*i.e.*, sensors made from the conductive graphite composite without the added liquid inclusions) using two sensing methods: a commercial charge integration circuit (MPR121), and an in-house designed charge integration circuit described in prior works[56] (Fig. 5). This second
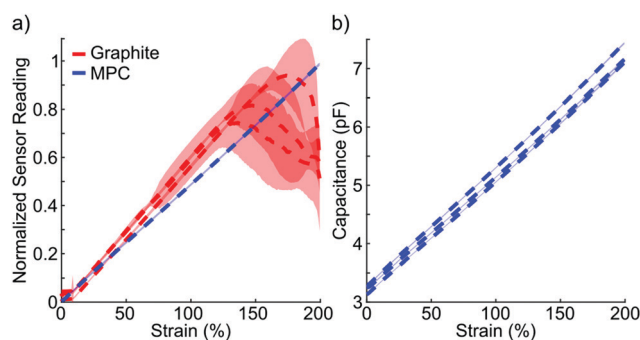

Fig. 5 Response of MPC strain sensors. (a) Comparison to SE–EIG capacitive sensors,[28] as measured using our charge-integration capacitance measuring circuit over 10 cycles. Normalized response is highly stable across all eight MPC sensors, while each of the three graphite sensors behaved similar over strains lower than $\sim$60% but had large inter- and intra-specimen variation at high strains. (b) MPC sensors stretched to 200% for 1000 cycles. Three sensors are plotted individually, showing high linearity and that they mainly differ in their intercept and slope. Dashed lines represent the mean over 10 cycles. Shaded regions in both plots represent ±1 standard deviation.

circuit was designed to work well with the relatively high resistance of the graphite sensors ($\sim$1–10 kΩ initially, and increasing to $\sim$100–1000 kΩ at 200% strain). The low resistance of MPC silicone was predicted to result in more stable sensor response, which was confirmed experimentally in Fig. 5a and Fig. S7 (ESI†). The low, stable resistance over large strains resulted in stable capacitance readings when MPC silicone was used as the electrode material. In contrast, the graphite sensors experienced cracking of their electrodes after around 60% strain, making them difficult to use as a strain sensor. MPC sensor readings S were normalized as $\bar{S} = \dfrac{S - S_0}{S_{\max} - S_{\min}}$, where $S_{\max}$ and $S_{\min}$ are the maximum and minimum reading over 10 cycles, respectively. Once this was done, the data from all eight MPC sensors that we tested collapsed into a single, linear response curve. Graphite sensors were normalized as $\bar{S} = \dfrac{S - S_0}{10\,000}$, and plotted individually due to the high inter-sensor and intra-sensor variability at strains greater than $\sim$60%. Raw data for each sensor are plotted individually in Fig. S7 (ESI†).

In addition to yielding stable readings, low electrode resistance makes it possible to utilize commercial off-the-shelf components. Here we used the commercial MPR121 circuit to measure capacitance over 1000 cycles to 200% strain, for three sensors separately (Fig. 5b). The relatively high resistance of the graphite sensors made them impossible to reliably read using the MPR121, giving an essentially flat curve after an inconsistent initial increase (Fig. S7, ESI†).

4.2 Solid state, damage resilient actuation

Recent developments in solid-state soft actuators have been boosted by the development of other liquid-inclusion silicone composites, such as the ethanol silicone blend developed by Miriyev *et al.*[24,57] This composite operates on a simple principle: heating the ethanol above its boiling temperature causes expansion *via* the liquid–gas transition. This in turn causes the silicone to increase in volume, up to 900%.[24] It is possible to harness this volumetric expansion inside of a McKibben-like mesh sleeve to control the direction of motion and the output forces, resulting in similar behavior to pneumatic actuators. The authors of the original work note that although the system can be rejuvenated by soaking in an ethanol bath for a period of time,[58] Joule heating the system with a Nichrome wire often results in localized burning of the silicone and eventual degradation of the silicone system beyond recovery.

Joule heating ethanol silicone with a soft, stretchable heater is difficult due to the large expansion of the system. One work has embedded kirigami-cut conductive fabrics inside of the ethanol silicone to distribute heat throughout the core.[59] We previously used our conductive SE–EIG composite as a Joule heating core inside these solid-state actuators to generate high contraction forces ($>$200 N),[25] but due to the low strain capacity of the initial heating composite (Fig. 2), we could only show contraction actuation.

Because the ethanol silicone composite is a closed-cell foam-like composite with millimeter sized ethanol capsules,[24] it is

relatively agnostic to damage. If the silicone is sliced or pierced, the material will continue to expand so long as it has a heat source. This adds an additional layer of complexity to heating the system: finding a heat source that is both compatible with the large expansion and also agnostic to damage received while operating.

Since the MPC is a bulk composite material, it can be damaged and continue to function. Fig. 6a shows an activated 4 $\times$ 16 cm strip of 60–40–1 MPC silicone (on a silicone backing layer) Joule heating before and after being cut with a blade. As long as the electrodes are reinstalled, the system continues to perform as it did prior to being damaged, with each segment showing uniform Joule heating.

As shown in Fig. 6b–d (and Video S3, ESI†), we created a directional-controlled, damage resilient expansion actuator by wrapping an ethanol silicone core in a fiber-reinforced silicone composite and then our MPC silicone. The fiber-reinforced silicone is similar to the material found here,[60] and prevents radial expansion of the ethanol-silicone tube. Fig. S8 (ESI†) shows that this can enable both extension and rotation actuation, although we focused on the high-strain extension actuation case, activated by the MPC layer wrapped around the outside.

Since the system is solid state (*i.e.*, actuating with no parts moving relative to each other), and MPC silicone is robust to damage, we added electrodes by simply piercing the tube with pins (see Fig. 6b and c insets). The pins provided a mechanical anchor for electrical clips, such that there was no concern of the clips loosing connection to the heater during operation. After applying extra liquid metal to reduce contact resistance between the pins and MPC silicone,[29] we Joule heated the external MPC to over 140 °C, causing the actuator to extend over 45% in length.

We demonstrated additional damage resilience by cutting the actuator in half and reactivating it (Fig. 6d). Since both the heater and the actuator were made of bulk materials, trimming them down with scissors only resulted in a shorter actuator. Adding new electrodes near the cut re-established electrical conductivity and the system could resume extension actuation *via* Joule heating.

Electrically interfacing with a highly deformable soft material is usually difficult (see Materials and methods for more discussion). Being able to run a pin through the entire system is a simple solution to a traditionally complex interfacing problem.[25] The pin becomes a robust connection point for rigid electronics that bring the power to the actuator (*i.e.*, copper wires or cables). Even though the system is undergoing large strains, the pins remain firmly lodged in the actuator. In this way, we gain the benefits demonstrated in our prior work,[25] with improved ability to interface with the electrical heater and an actuator that can extend instead of just contract.

4.3 Multi-directional single-channel pneumatic soft actuators

In addition to functioning as the heat source for a liquid-to-gas phase change (driving the silicone actuator), MPC silicone can also induce solid-to-liquid phase changes, resulting in silicones with a variable material modulus. For example, it has been
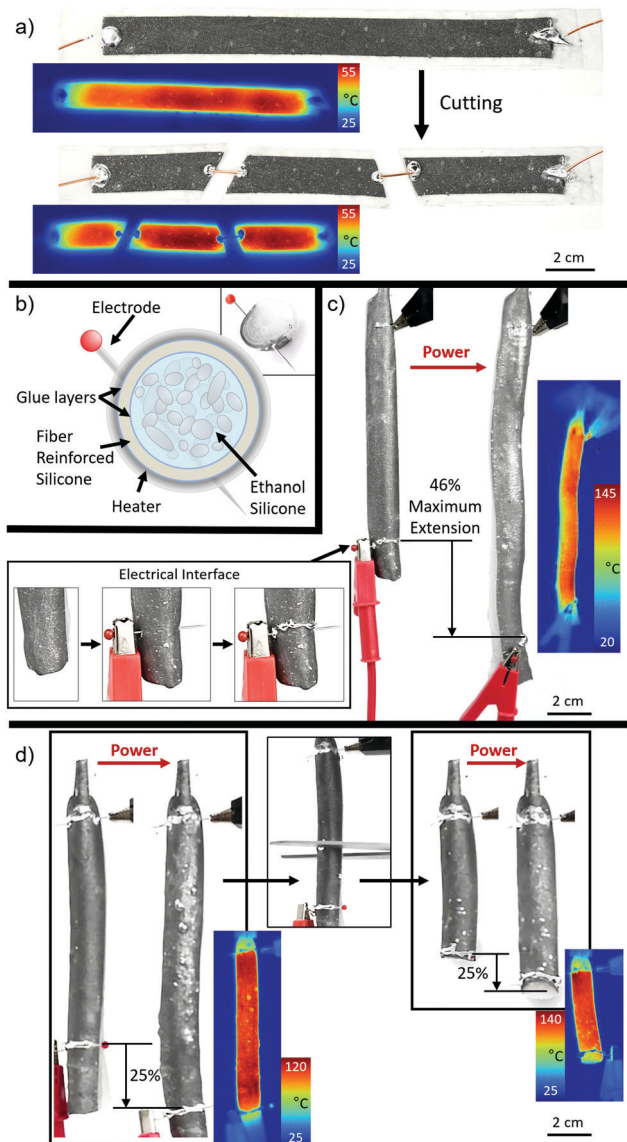
Fig. 7 MPC silicone applied as a heater on a stretchability-changing pneumatic bladder. (a) Front view of the pneumatic bladder, along with an IR image showing the MPC increasing the temperature sufficiently to melt the metal particles inside the Field's metal silicone (FMSi) bladder wall. (b) Cross-sectional diagram of the actuator. (c) Still frames (both IR and visible light) of the trajectory-changing pneumatic bladder cycling through different trajectories enabled by selectively heating the bladder's walls.

Fig. 6 MPC silicone damage resilience. (a) MPC silicone shown to be conductive before and after being cut into pieces. (b) Cross-sectional diagram of the actuator system, with photograph inset of the same. (c) Joule heating the MPC boils the ethanol trapped in the silicone core. The resulting expansion is controlled by the fiber reinforced silicone wrap, resulting in a 46% maximum elongation of the actuator. (Inset) The solid-state nature of the system allows for easy electrode creation by piercing the system with a pin. (d) Both the actuator and the MPC silicone heater are agnostic to being cut in half, and, once the electrodes are restored, the system can continue to produce a 25% elongation.

shown that when Field's metal is added as a composite filler into a thin film of silicone, and attached to a pneumatic bladder, selectively heating the walls allows for a trajectory change as the pneumatic bladder inflates.[26,61] This Field's metal silicone composite (FMSi) experiences a change in its stretchability when the Field's metal is melted (T_m = 62 °C). Additionally, it has been shown that this phase transition allows the FMSi to experience a type of "shape locking". If the silicone is cooled while stretched, the inclusions will
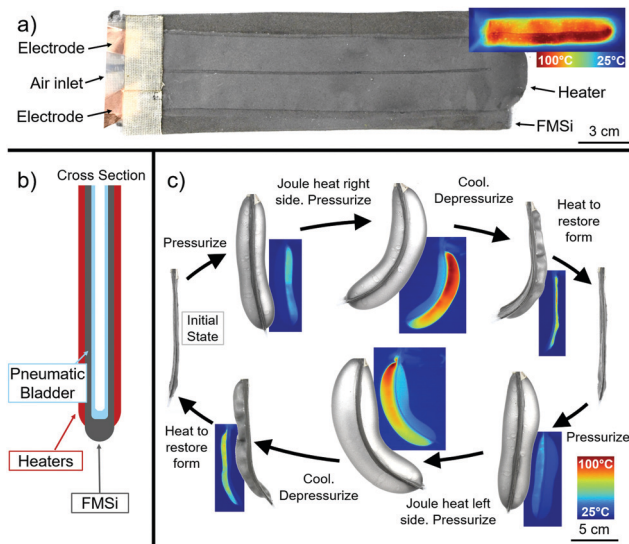
freeze and attempt to hold their deformed shape. In both prior examples though, an external heat source was needed.

To create a self-activating trajectory changing actuator, we prepared a demonstration similar to that shown by Buckner *et al.*,[26] with an additional layer of pre-activated 60–40–1 MPC silicone on the outside in order to allow for on-demand Joule heating of the FMSi walls. Fig. 7a shows a front view of the bladder, with one of the MPC heaters clearly visible in a U-shape on top of the FMSi. We chose this shape to allow for heating of the whole surface while also enabling us to access both ends of the heater from the top of the pneumatic bladder. We attached heaters to both sides of the bladder so that we could independently control the stretchability of each side (Fig. 7b). Stiffness control is derived from thermally controlling the phase of the Field's metal particles (solid particles below T_m, liquid inclusions above T_m): melted particles increase the composite's ability to stretch.

By patterning material stiffness on the surface of an inflatable actuator, the trajectory of inflation can be changed on-demand. Fig. 7c shows that selectively softening one side of the bladder (by applying current to the co-located stretchable Joule heater MPC sheet) influenced actuator bending in the stiff-material direction. Selectively softening the opposite side of the bladder influenced bending in the opposite direction. This demonstration shows that it is possible to achieve at least three different actuation trajectories in a pneumatic bladder (straight, bending left, and bending right) using only a single air input. The high-strain, highly electrically uniform MPC silicone on the outside of the bladder enabled Joule heating of the bladder's walls, yielding a way to electrically control the actuator's inflation trajectory.

4.4 Pneumatic bladder trajectory change with sensor feedback

Embedding sensors into pneumatic actuators is difficult due to the noise generated by the pneumatic inflation against the sensor. Often, researchers resort to using flexible (but not stretchable) sensors.[19,62,63] Stretchable sensors added to the system require careful planning of sensor location so as to reduce the noise generated by the pneumatic inflation on the sensor's response to the curvature in the actuator.[64] In this work, our MPC silicone is capable of withstanding high strains and, when used as a capacitive strain sensor, provides a low-noise signal. In Fig. 7, we show that the synergy between heating and strain capabilities allowed the variable-trajectory actuator to sense its motion. Specifically, we added a second layer of MPC onto the outside of the bladder (see diagram and cross-sections in Fig. 8a), and observed the sensor response as the system underwent inflation, trajectory change, and shape recovery (Fig. 8b, and Video S4, ESI†).

To minimize system complexity, we used the heater MPC silicone layer as the ground plane of the capacitive sensor (Fig. 8a). This allowed us to reduce the thickness to approximately 3.25 mm per wall. Each layer of MPC silicone on each wall is relatively thin (120 μm each, for a total of ∼240 μm), while the remaining thickness came from the glue layer between the MPC silicone and the FMSi, in addition to the dielectric layer. For this reason, we used a stiffer silicone for the FMSi, so that the glue layer's thickness would not dominate the wall's stretchability (see the Materials and methods section for more details). Note that the FMSi is not conductive, and so it could not be used as part of the sensor.

Fig. 8b shows the data, as well as the experimental steps used to test the sensor response. First, the system was inflated partially, to engage the sensors. Then, we heated up the right wall (from the perspective shown throughout Fig. 8), using the MPC heater. As the Field's Metal particles melted, the system subtly shifted the direction it was pointing and both sensors on the bladder responded to the positional shift in the expected manner: as the right wall heated up and softened, the whole wall expanded from the constant air pressure in the bladder. This caused the corresponding sensor to increase its capacitance. Furthermore, the sensor on the left (the cold wall) dropped its capacitance as the wall was able to contract slightly from its initial stretched state as the softer right wall expanded further.

After initiating trajectory change, we followed a similar method to that of the demonstration in Fig. 7c. First, we inflated the actuator the rest of the way, observing that the sensor on the heated wall experienced a much greater change in capacitance. Then, we cooled the wall down and deflated the actuator, noting that the sensors detected the pressure change. Once the bladder was deflated, the right wall was holding an "expanded" shape, and so the sensor did not return to its original value. We used the MPC silicone heater to re-melt the Field's Metal particles in that wall and the sensor values dropped back to their relaxed states. Since the pressure in the bladder was in equilibrium with atmosphere, the left hand sensor did not respond to the heating and restoration of the original shape, as the left wall was already relaxed. This sequence showed that it is possible to use MPC silicone to
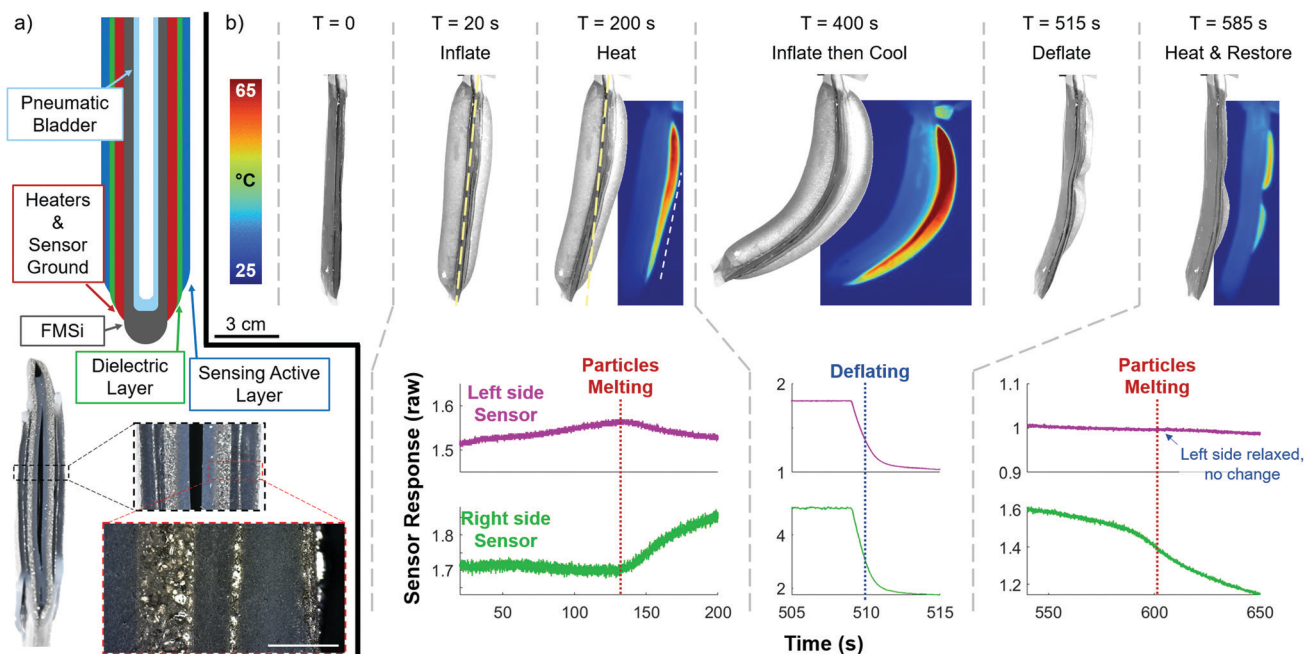

Fig. 8 MPC silicone applied as a heater and a sensor on a stiffness–changing pneumatic bladder. (a) Schematics and photographs of the cross section of the pneumatic bladder. Inset scalebar is 1 mm. Silicone glue layers are not shown in the schematic unless they serve an additional functional purpose (b) visible light and IR photographs of the sensorized bladder at various times, along with graphs of the raw sensor response as the system undergoes both temperature and pressure changes.

create a thin, sensorized, trajectory changing, single-air-input pneumatic bladder.

5 Conclusions

We have presented a liquid-composite silicone with a high, spatially uniform conductivity (as demonstrated by Joule heating), which is robust to high deformations (200% strain) at high cycles of use (over 10 000 cycles), and has only a 2× increase in resistance at 200% strain. All these properties together in a thin film enable many applications, some of which we demonstrated, including a stretchable Joule heater and a capacitive sensor responsive to strains up to 200%. We also showed both the heater and sensor being applied to drive high-strain linear actuation and stretchability change in high-deformation, shape-locking silicone composites. Furthermore, we showed that this material is robust to damage—if the system is cut, one must simply add a new electrode and it will continue to function as normal—a potentially impactful trait for a new soft robotic material.

In the future, we hope to continue to explore new activation methods, as well as new rigid filler materials. We do this with the goal of slightly increasing the overall material resistivity while maintaining the current manufacturing reliability and uniform conductivity. A higher resistivity would help us to scale-up the system to larger areas (geometrically reducing the resistance), so that we can Joule heat the MPC silicone using higher voltages and lower currents. By choosing a different activation stimulus (such as freeze activating[35]) or non-conductive rigid fillers, it may be possible to reduce the volume fraction of liquid metal in the MPC silicone so that the system could have both a lower mass and a higher resistance, while still maintaining a highly reliable activation mechanism.

6 Materials and methods

6.1 Materials and material preparation

6.1.1 Silicone. Ecoflex 50 (Smooth-On Inc.) was used as the primary silicone elastomer for all experiments, as both matrix for the liquid inclusions and the reinforcing backing layer. Dragonskin 10 (Smooth-On Inc.) was used as the matrix silicone for the Field's metal silicone (FMSi), to ensure that the stiffness of the FMSi sheets dominated the effects of the glue layers in the composite system.

6.1.2 Composite fillers. Expanded intercalated graphite (EIG) was prepared using the techniques detailed in previous works.[28,29] Expandable graphite (Sigma-Aldrich) was roasted at 800 °C, added to a carrier solvent (cyclohexane, BDH1111, VWR), then sonicated to break the graphite into microscopic, graphene-like particles. Once the excess solvent was decanted, the solution was weighed and mixed into silicone precursors.

Eutectic gallium–indium (eGaIn) was prepared in-house by mixing 1 kg of indium (99.9% pure, RotoMetals) with 3 kg of gallium (99.99% pure, RotoMetals) in a beaker heated to 150 °C overnight on a hot plate. Once mixed, any residual solids were

scraped off the top of the liquid alloy, then the alloy was allowed to cool back down to room temperature. Once cooled, the eutectic components were decanted off from the remaining residual solids and stored for later use.

Field's metal alloy (Roto144F Low Melt Fusible Ingot Alloy, RotoMetals) was reduced into microscopic filler particles (size range 100–375 μm) using the same techniques detailed in previous works.[26] The alloy was melted in a beaker of hot water (80 °C), mixed with a homogenizer for 2.5 min to break the liquid alloy into particles. When the cycle finished, cold water was immediately added to reduce the ambient temperature around the particles to less than 62 °C, solidifying the particles and preventing them from fusing. The particles then sink to the bottom and are sieved out of the water, dried, and stored for later use.

6.1.3 Composites preparation. LM–SE–EIG multiphase composite (MPC) silicone was manufactured in the following steps: (1) both parts of a two-part silicone elastomer were premixed, ensuring a proper 1-to-1 ratio of the two components. (2) LM was carefully shear-mixed with silicone elastomer manually for several minutes, until no visible droplets of LM remained. (3) The EIG/cyclohexane solution was added to the LM–SE mixture in sufficient quantity so that the amount of EIG remaining in the system after the cyclohexane evaporated would be the desired volumetric ratio. (4) Once all parts were mixed together, if the system's viscosity was higher than desired, additional cyclohexane was added. A mask was cut out of 20 μm thick paper, and placed on a flat acrylic sheet. The final composite mixture was poured at one end of the mask and coated over the whole mask using custom made drawbars of 300 μm, 500 μm, and 1 mm thickness. After the mask was removed, the composite was left at room temperature to dry and then cure. At this point, the composite could be lifted and removed from the acrylic, or the first silicone elastomer reinforcing backing layer could be draw-coated over the top, depending on the sample being made.

LM–SE, and SE–EIG were manufactured using the same steps as the MPC silicone, withholding only the material that needed to be omitted.

Ethanol silicone was prepared using the same techniques detailed in previous works.[25] Parts A and B of a two part silicone and pure ethanol were mixed in a 2–2–1 ratio (by volume) resulting in a final composite of 20 vol% ethanol. The silicone was mixed slowly at first by hand to trap the ethanol in small bubbles internal to the system (approximately 1 minute of mixing). Once all the liquid ethanol on top of the silicone was mixed in, the composite was mixed at 2000 rpm in a planetary centrifugal mixer machine (Thinky Mixer, Thinky, USA) for an additional minute in order to reduce the size of the ethanol bubbles. Then, the silicone was cast into its desired shape (a tube) and sealed to prevent the ethanol from escaping during the curing process.

The fiber reinforced silicone was manufactured using methods similar to those recorded in previous works.[60] A 0.3 mm diameter polyester fiber (sewing thread) was wound around a large drum (6 in [15.24 cm] diameter) with a spacing of approximately 0.8 mm

between fiber centers. Then, while the drum continued to rotate, uncured silicone was coated over the fibers using a flat surface to ensure an even coating of silicone over all the fibers. Finally, the drum was allowed to spin gently for several hours as the silicone cured to ensure a uniform thickness of silicone. Once cured, the sheet was removed from the drum. This resulted in a thin sheet of fiber reinforced silicone (0.75 mm thick).

The directional controlled solid-state actuators were made by cutting the fiber reinforced silicone into appropriate sizes, wrapping it twice around the ethanol silicone tubes, and gluing it together with additional uncured silicone.

Field's metal silicone was manufactured by mixing 30% Field's Metal particles by volume into Part A and B of Dragon-skin 10 (SMooth-On Inc.). The uncured composite paste was then coated on a flat acrylic sheet with a 1 mm drawbar. After curing for 4 hours, appropriate sized sheets were cut and glued to each side of the silicone pneumatic bladder using an additional thin layer of silicone.

6.2 Mechanical and electrical characterization

Elongation at break and cyclic loading of LM–SE–EIG rectangular specimens (40 mm gauge length by 10 mm width and between 0.2 to 0.4 mm thickness) were evaluated in Instron 3345 testing machine equipped with a 50 N load cell (Fig. 3d and e). Electrical characterization specimens included active dimensions of 20 mm × 10 mm × 0.2–0.4 mm thickness, and were supported by an additional backing layer of pure silicone to prevent premature failure. Resistance change in the activation process of MPC silicones (Fig. 3f) was evaluated by measuring the voltage across the specimens while simultaneously straining them in the Instron testing machine. We also measured the resistance of two samples (1-sided and 2-sided backing layer) with 50–50–2 composition over a period of 90 days (Fig. S9, ESI†). After an initially sharp rise in resistance over the first 7 days, both samples settled into a very gradual increase for the remaining time.

6.3 Electrodes and interfaces

For the simplest demonstrations, a bead of LM was placed on the surface of the MPC silicone and copper wires gently connected to the beads. The bead of LM reduced contact resistance between the copper wires and the MPC,[29] enabling the demonstration of uniform conductivity through the MPC itself.

For the more detailed demonstrations (including the activation testing done in a vertical testing apparatus (Fig. 3), as well as the cyclic testing (Fig. 4)), a low-resistance, high stretchable electrode is a technical challenge. Often, the biggest challenge is the interface between the soft, high-deformation material and inextensible copper wires.[65] To create most of the electrical interfaces in this paper, we followed a similar tactic used in our previous works[29] where a bead of LM was placed directly on the MPC, and a copper wire (or film) was interfaced into that bead. Then, the electrode was sealed with silicone and an inextensible layer (porous muslin fabric tabs) that significantly reduced the strains in the joint between the liquid metal

and the copper. This method is also supported by recent literature.[66]

The only deviance from these two methods was in the solid-state actuator demonstration, where a pin was simply driven through the actuator, and a small layer of LM wrapped around the MPC to create an electrode with uniform conductivity along the entire circumference of the heating skin.

6.4 Capacitive strain sensors

Two types of three-layer sensors (electrode, dielectric, electrode) were manufactured using a conductive SE–EIG composite made with 10 wt% EIG,[28] and the new MPC as electrodes materials. The active region of both types was 10 cm by 1 cm.

Two capacitance measuring devices were used: MPR121 (by NXP Semiconductor, used as a component in a breakout board sold by Adafruit, Inc.), and a customized charge-integration circuit developed by our lab (described in ref. 28, theory elaborated in ref. 56). This custom circuit charged the sensors' top electrode for a constant time, then measured the time it took to discharge through a 10 M resistor to a known voltage reference. Importantly, the MPR121 is designed for capacitors with low electrode resistance, while the custom circuit was designed to be used with capacitive sensors with a wide range of resistances. Three test protocols were considered: (1) the sensors at resting length (ε = 0%) with no noise intentionally injected; (2) the sensors at resting length with a DC motor placed 3 cm away and ran at 12 V (resulting in ~100 rpm; item number 2826 from Pololu); (3) the sensors with no noise intentionally injected, pulled (using an Instron 3345) at 200 mm min^{-1} until 200 mm (ε = 200%) for 10 cycles. Data were collected for all combinations of sensor type, measuring device, and these three test protocols. Finally (test protocol 4), three MPC sensors were tested with the MPR121 and pulled at 200 mm min^{-1} until 200 mm for 1000 cycles. Key findings were presented in the main text, while noise characterization and complete raw data are presented in the ESI.†

Conflicts of interest

There are no conflicts to declare.

Acknowledgements

References

1 F. Ilievski, A. D. Mazzeo, R. F. Shepherd, X. Chen and G. M. Whitesides, *Angew. Chem., Int. Ed.*, 2011, **50**, 1930–1935.

2 E. Brown, N. Rodenberg, J. Amend, A. Mozeika, E. Steltz, M. R. Zakin, H. Lipson and H. M. Jaeger, *Proc. Natl. Acad. Sci. U. S. A.*, 2010, **107**, 18809–18814.

3 F. Connolly, D. A. Wagner, C. J. Walsh and K. Bertoldi, *Extreme Mech. Lett.*, 2019, **27**, 52–58.

4 C. Walsh, *Nat. Rev. Mater.*, 2018, **3**, 78–80.

5 Q. Shi, J. Sun, C. Hou, Y. Li, Q. Zhang and H. Wang, *Adv. Fiber Mater.*, 2019, **1**, 3–31.

6 T. G. Thuruthel, Y. Ansari, E. Falotico and C. Laschi, *Soft Robot.*, 2018, **5**(2), 149–163.

7 Y. Gao, L. Yu, J. C. Yeo and C. T. Lim, *Adv. Mater.*, 2020, **32**, 1902133.

8 I. D. Joshipura, M. Finn, S. T. M. Tan, M. D. Dickey and D. J. Lipomi, *MRS Bull.*, 2017, **42**, 960–967.

9 D. Kim, J. Kwon, S. Han, Y.-L. Park and S. Jo, *IEEE/ASME Trans. Mechatronics*, 2019, **24**, 56–66.

10 D. Hughes, C. Heckman and N. Correll, *Int. J. Robot. Res.*, 2019, **38**, 1338–1351.

11 Y. Zhao, A. Kim, G. Wan and B. C. K. Tee, *Nano Convergence*, 2019, **6**, 25.

12 N. Matsuhisa, X. Chen, Z. Bao and T. Someya, *Chem. Soc. Rev.*, 2019, **48**, 2946–2966.

13 D. F. Fernandes, C. Majidi and M. Tavakoli, *J. Mater. Chem. C*, 2019, **7**, 14035–14068.

14 D. C. Kim, H. J. Shim, W. Lee, J. H. Koo and D. Kim, *Adv. Mater.*, 2020, **32**, 1902743.

15 S. Y. Kim, Y. Choo, R. A. Bilodeau, M. C. Yuen, G. Kaufman, D. S. Shah, C. O. Osuji and R. Kramer-Bottiglio, *Sci. Robot.*, 2020, **5**, eaay3604.

16 S. Hong, H. Lee, J. Lee, J. Kwon, S. Han, Y. D. Suh, H. Cho, J. Shin, J. Yeo and S. H. Ko, *Adv. Mater.*, 2015, **27**, 4744–4751.

17 Y. Hu, T. Zhao, P. Zhu, Y. Zhu, X. Shuai, X. Liang, R. Sun, D. D. Lu and C.-P. Wong, *J. Mater. Chem. C*, 2016, **4**, 5839–5848.

18 E. J. Markvicka, M. D. Bartlett, X. Huang and C. Majidi, *Nat. Mater.*, 2018, **17**, 618.

19 R. A. Bilodeau, M. C. Yuen, J. C. Case, T. L. Buckner and R. Kramer-Bottiglio, 2018 IEEE/RSJ International Conference on Intelligent Robots and Systems (IROS), 2018, pp. 1–8.

20 S. Choi, S. I. Han, D. Kim, T. Hyeon and D.-H. Kim, *Chem. Soc. Rev.*, 2019, **48**, 1566–1595.

21 S. Choi, S. I. Han, D. Jung, H. J. Hwang, C. Lim, S. Bae, O. K. Park, C. M. Tschabrunn, M. Lee, S. Y. Bae, J. W. Yu, J. H. Ryu, S.-W. Lee, K. Park, P. M. Kang, W. B. Lee, R. Nezafat, T. Hyeon and D.-H. Kim, *Nat. Nanotechnol.*, 2018, **13**, 1048–1056.

22 C. Pan, Y. Ohm, J. Wang, M. J. Ford, K. Kumar, S. Kumar and C. Majidi, *ACS Appl. Mater. Interfaces*, 2019, **11**, 42561–42570.

23 N. Matsuhisa, M. Kaltenbrunner, T. Yokota, H. Jinno, K. Kuribara, T. Sekitani and T. Someya, *Nat. Commun.*, 2015, **6**, 1–11.

24 A. Miriyev, K. Stack and H. Lipson, *Nat. Commun.*, 2017, **8**, 596.

25 R. A. Bilodeau, A. Miriyev, H. Lipson and R. Kramer-Bottiglio, 2018 IEEE International Conference on Soft Robotics (RoboSoft), Livorno, Italy, 2018, pp. 288–294.

26 T. L. Buckner, M. C. Yuen, S. Y. Kim and R. Kramer-Bottiglio, *Adv. Funct. Mater.*, 2019, **29**, 1903368.

27 M. J. Ford, C. P. Ambulo, T. A. Kent, E. J. Markvicka, C. Pan, J. Malen, T. H. Ware and C. Majidi, *Proc. Natl. Acad. Sci. U. S. A.*, 2019, **116**, 21438–21444.

28 E. L. White, M. C. Yuen, J. C. Case and R. K. Kramer, *Adv. Mater. Technol.*, 2017, **2**, 1700072.

29 R. A. Bilodeau, M. C. Yuen and R. Kramerâ-Bottiglio, *Adv. Mater. Technol.*, 2019, **4**, 1900276.

30 M. D. Bartlett, A. Fassler, N. Kazem, E. J. Markvicka, P. Mandal and C. Majidi, *Adv. Mater.*, 2016, **28**, 3726–3731.

31 M. D. Bartlett, N. Kazem, M. J. Powell-Palm, X. Huang, W. Sun, J. A. Malen and C. Majidi, *Proc. Natl. Acad. Sci. U. S. A.*, 2017, **114**, 2143–2148.

32 H. Wang, Y. Yao, X. Wang, L. Sheng, X.-H. Yang, Y. Cui, P. Zhang, W. Rao, R. Guo, S. Liang, W. Wu, J. Liu and Z.-Z. He, *ACS Omega*, 2019, **4**, 2311–2319.

33 C. Pan, E. J. Markvicka, M. H. Malakooti, J. Yan, L. Hu, K. Matyjaszewski and C. Majidi, *Adv. Mater.*, 2019, **31**, 1900663.

34 Y. Wang, G. Sun, J. Yang, L. Zhang and J. Zhou, *AIP Adv.*, 2020, **10**, 015016.

35 L.-Y. Zhou, J.-Z. Fu, Q. Gao, P. Zhao and Y. He, *Adv. Funct. Mater.*, 2020, **30**, 1906683.

36 R. Tutika, S. H. Zhou, R. E. Napolitano and M. D. Bartlett, *Adv. Funct. Mater.*, 2018, **28**, 1804336.

37 M. Tavakoli, M. H. Malakooti, H. Paisana, Y. Ohm, D. Green Marques, P. Alhais Lopes, A. P. Piedade, A. T. de Almeida and C. Majidi, *Adv. Mater.*, 2018, **30**, 1801852.

38 H. Sun, Z. Han and N. Willenbacher, *ACS Appl. Mater. Interfaces*, 2019, **11**, 38092–38102.

39 J. Wang, G. Cai, S. Li, D. Gao, J. Xiong and P. S. Lee, *Adv. Mater.*, 2018, **30**, 1706157.

40 J. Park, S. Wang, M. Li, C. Ahn, J. K. Hyun, D. S. Kim, D. K. Kim, J. A. Rogers, Y. Huang and S. Jeon, *Nat. Commun.*, 2012, **3**, 1–8.

41 S. Zhu, J.-H. So, R. Mays, S. Desai, W. R. Barnes, B. Pourdeyhimi and M. D. Dickey, *Adv. Funct. Mater.*, 2013, **23**, 2308–2314.

42 C. Thrasher, Z. Farrell, N. Morris, C. Willey and C. Tabor, *Adv. Mater.*, 2019, **31**, 1903864.

43 J. C. Case, E. L. White and R. K. Kramer, *Soft Robot.*, 2015, **2**, 80–87.

44 N. Kazem, T. Hellebrekers and C. Majidi, *Adv. Mater.*, 2017, **29**, 1605985.

45 D. Yang, B. Mosadegh, A. Ainla, B. Lee, F. Khashai, Z. Suo, K. Bertoldi and G. M. Whitesides, *Adv. Mater.*, 2015, **27**, 6323–6327.

46 D. M. Bigg, *Adv. Polym. Technol.*, 1984, **4**, 255–266.

47 D. Sritharan and E. Smela, *Polymers*, 2016, **8**, 400.

48 K. Chu, S.-C. Lee, S. Lee, D. Kim, C. Moon and S.-H. Park, *Nanoscale*, 2014, **7**, 471–478.

49 J. Jang, B. G. Hyun, S. Ji, E. Cho, B. W. An, W. H. Cheong and J.-U. Park, *NPG Asia Mater.*, 2017, **9**, e432.

50 A. Tairych and I. A. Anderson, *Soft Robot.*, 2019, **6**, 389–398.

51 Q. Gao, J. Zhang, Z. Xie, O. Omisore, J. Zhang, L. Wang and H. Li, *J. Mater. Sci.*, 2019, **54**, 5187–5223.

52 J. W. Booth, D. Shah, J. C. Case, E. L. White, M. C. Yuen, O. Cyr-Choiniere and R. Kramer-Bottiglio, *Sci. Robot.*, 2018, **3**, 1–10.

53 M. Amjadi, K.-U. Kyung, I. Park and M. Sitti, *Adv. Funct. Mater.*, 2016, **26**, 1678–1698.

54 K. Sim, Z. Rao, F. Ershad and C. Yu, *Adv. Mater.*, 2020, **32**, 1902417.

55 B. O'Brien, T. Gisby and I. A. Anderson, *Proceedings of SPIE 9056, Electroactive Polymer Actuators and Devices (EAPAD)*, 2014, p. 905618.

56 E. L. White, J. C. Case and R. Kramer-Bottiglio, *Soft Robot.*, 2018, **5**, 36–53.

57 A. Miriyev, G. Caires and H. Lipson, *Mater. Des.*, 2018, **145**, 232–242.

58 A. Miriyev, C. Trujillo, G. Caires and H. Lipson, *MRS Commun.*, 2018, **8**, 556–561.

59 M. Cartolano, B. Xia, A. Miriyev and H. Lipson, *Actuators*, 2019, **8**, 9.

60 S. Y. Kim, R. Baines, J. Booth, N. Vasios, K. Bertoldi and R. Kramer-Bottiglio, *Nat. Commun.*, 2019, **10**, 1–8.

61 A. M. Nasab, A. Sabzehzar, M. Tatari, C. Majidi and W. Shan, *Soft Robot.*, 2017, **4**, 411–420.

62 K. Elgeneidy, G. Neumann, M. Jackson and N. Lohse, *Front. Robot. AI*, 2018, **5**, 2.

63 S. Ozel, E. H. Skorina, M. Luo, W. Tao, F. Chen, Y. Pan and C. D. Onal, 2016 IEEE International Conference on Robotics and Automation (ICRA), 2016, pp. 4963–4968.

64 R. A. Bilodeau, E. L. White and R. K. Kramer, 2015 IEEE/RSJ International Conference on Intelligent Robots and Systems (IROS), 2015, pp. 2324–2329.

65 O. D. Yirmibesoglu and Y. Menguc, 2016 IEEE International Conference on Automation Science and Engineering (CASE), 2016, pp. 798–804.

66 M. Li, Y. Wu, L. Zhang, H. Wo, S. Huang, W. Li, X. Zeng, Q. Ye, T. Xu, J. Luo, S. Dong, Y. Li, H. Jin and X. Wang, *Nanoscale*, 2019, **11**, 5441–5449.